The effect of silver coating on magnetic properties of oxygen-stabilized tetragonal Ni nanoparticles prepared by chemical reduction

2007 J. Phys.: Condens. Matter 19 346220

(http://iopscience.iop.org/0953-8984/19/34/346220)

IOP PUBLISHING JOURNAL OF PHYSICS: CONDENSED MATTER

J. Phys.: Condens. Matter **19** (2007) 346220 (16pp) doi:10.1088/0953-8984/19/34/346220

The effect of silver coating on magnetic properties of oxygen-stabilized tetragonal Ni nanoparticles prepared by chemical reduction

Aparna Roy[1,4], V Srinivas[1], S Ram[2] and T V Chandrasekhar Rao[3]

[1] Department of Physics and Meteorology, Indian Institute of Technology, Kharagpur-721302, India
[2] Materials Science Centre, Indian Institute of Technology, Kharagpur-721302, India
[3] Technical Physics and Prototype Engineering Division, Bhabha Atomic Research Centre, Bombay-400085, India

E-mail: aparna@phy.iitkgp.ernet.in

Received 19 February 2007, in final form 28 June 2007
Published 26 July 2007
Online at stacks.iop.org/JPhysCM/19/346220

Abstract

Ni–nickel oxide and Ni–Ag nanoparticles with core–shell morphology have been synthesized by a simple two-step chemical route. It involves the reduction of Ni^{2+} cations to Ni particles with sodium borohydride ($NaBH_4$) in aqueous solution, followed by coating part of the sample with a surface layer of silver. The coating was accomplished via a simple transmetallation reaction, $Ni + 2Ag^{+} \rightarrow 2Ag + Ni^{2+}$, in aqueous $AgNO_3$ solution at room temperature. Particles left uncoated have a thin spontaneous surface oxide layer of nickel oxide, presumably non-stoichiometric, as a passivating layer. From x-ray diffraction patterns, the Ni in as-prepared samples, both coated and uncoated, has been identified as being in a tetragonal crystal structure, different from its usual fcc form. This structural modification is due to the presence of interstitial oxygen atoms in the Ni lattice, and results in appreciably modified magnetic properties in this new phase of Ni, for example a linear non-hysteretic magnetization response with applied field at room temperature. A comparative magnetic study of the uncoated and silver coated Ni particles exemplifies the role played by the Ag shell in modifying the magnetic properties of the coated sample. This is evident from the smaller coercivity and remnant magnetization in the hysteresis loop at 5 K in the case of the Ag coated as-prepared sample, larger magnetic moment but smaller saturation magnetization and susceptibility of the Ag coated air annealed sample, and higher blocking temperature for this sample in comparison to the uncoated counterparts. These features have been coherently explained on the basis of the structural modifications induced in these samples by Ag coating.

[4] Author to whom any correspondence should be addressed.

1. Introduction

In recent years considerable attention has been devoted to the study of ultrafine magnetic particles, due to their rich physical properties as well as extensive prospects for electronic and magnetic device applications [1–3]. Magnetic nanomaterial research has generally been focused on understanding the interactions between magnetic entities, modelling of interaction effects, and comprehension of the role played by the surface on the magnetic properties of these materials. For such fundamental studies, nanosized particles of ferromagnetic transition metals (TM) such as Fe, Co and Ni provide better model systems in comparison to complex alloys and compounds since in the latter class of materials it is difficult to separate out various effects that contribute to the magnetic properties [4, 5]. However, synthesis of free-standing nanoparticles is beset with problems such as surface oxidation and the formation of macroscopic sized agglomerates, leading to properties different from those of independent nanoparticles.

The average size and the shape of nanoparticles strongly depend on the parameters involved in the method of preparation. Although spherical particles can be obtained by distinct growth techniques, namely, cluster beam deposition and the chemical reduction method, quite often they result in particles with a spontaneous surface oxide (SSO) layer [6–9]. However, such materials with core–shell (metal–metal oxide) morphology are of interest in their own right and have been the subject of extensive research in the past [4–9]. For example, a ferromagnetic TM core surrounded by an antiferromagnetic transition metal oxide (TMO) shell forms a magnetic bilayer structure which is a source of a large effective additional anisotropy, leading to a marked improvement in the thermal stability of the moments of the ferromagnetic nanoparticles [9]. But a magnetic passivation layer on the surface potentially alters the magnetic properties of the particle by weakening the exchange interactions of the surface atoms with the surrounding ones.

One of the ways to evade the formation of SSO layer is to synthesize and encapsulate the nanoparticles with inert, non-magnetic passivation layers of insulators (Al_2O_3 and SiO_2) or noble metals (Ag, Pt, Au) [10–14]. These structures are of considerable interest for many applications requiring small particles having high magnetic susceptibility. The metallic magnetic component would provide excellent magnetic sensitivity for interaction with an external field while the passivated coating would provide a surface that could easily be functionalized.

Transition metal elements such as Fe, Co and Ni are immiscible with Ag in both solid and liquid states, which (Ag) therefore is ideal for forming passivating surface layers around nanoparticles of these metals. These binary combinations are expected to form perfect core–shell structures as no alloying takes place even at elevated temperatures (there are, however, some reports indicating atomic level mixing in amorphous thin films to be possible [15]). Furthermore, TM–Ag systems are also one of the representative binaries used to form heterogeneous granular structures (Fe, Co or Ni embedded in Ag matrix) that exhibit GMR (giant magneto resistance) [16–18]. On the theoretical front the granular structures are simpler and more amenable for modelling than the complex structures obtained by alternately depositing layers of non-lattice-matched materials.

Among transition metal elements, research in bulk as well as nanoscale dimensions of Ni and NiO has been pursued with a renewed interest because of their possible use as viable materials for spintronics applications [4–7, 9]. In fact NiO has become a vital component of spin valve structures. However controlled surface passivation of the particles is essential in order to achieve suitable properties for different applications. Therefore, preparation of core–shell structures of ‘Ni (core) and Ag or NiO (shell)’ would not only render the Ni core more robust, chemically, but also provide us a way to manipulate the surface properties of these nanoparticles.

In this paper we report a comparative study of the structure and magnetic properties of fine Ni particles with either a SSO layer or Ag coating, prepared by the borohydride reduction method. The effect of shell on the magnetic properties has been investigated in detail. The stability of the particles has been examined in ambient conditions and in controlled atmosphere.

2. Experimental details

Ni fine particles were prepared by reducing the salt $NiCl_2{\cdot}6H_2O$ with sodium borohydride ($NaBH_4$) in aqueous solution, ambient atmosphere and room temperature as reported earlier [19, 20]. 200 ml of 1 M aqueous $NaBH_4$ was added dropwise to 500 ml of 0.1 M aqueous $NiCl_2{\cdot}6H_2O$ solution in a beaker with constant magnetic stirring, resulting in an instantaneous exothermic reaction and the formation of black slurries of fine Ni particles. The dropwise addition controls the reaction, maintaining the average temperature of the solution at ∼300 K. After the $Ni^{2+} \rightarrow Ni$ reaction, the sample (slurries of Ni fine particles) was filtered and washed thoroughly with distilled water to remove NaCl and other by-product impurities. This was followed by washing with acetone to remove the water. A part of the powder was taken out and dried in ambient conditions (air, room temperature) resulting in the formation of a stable surface passivation layer of nickel oxide (probably non-stoichiometric) around the particles. This sample will henceforth be referred as uncoated Ni (uc-Ni).

The remaining part of the powder was added to an aqueous solution of 2 M $AgNO_3$ (silver nitrate) and magnetically stirred. The colour of the $AgNO_3$ solution immediately changed to brownish yellow indicating coating of the Ni particles by silver. The silver coating was accomplished via a transmetallation reaction, namely $Ni + 2Ag^+ \rightarrow 2Ag + Ni^{2+}$ occurring at the surface of the Ni particles, due to which the surface Ni gets replaced by a uniform layer of Ag[5]. The formation of discrete islands of Ag on the surface of Ni nanoparticles may be ruled out since all Ni atoms on the surface layers of the Ni core are consumed in the transmetallation reaction, forming metallic Ag at their sites. Silver-coated nickel powders so produced (here after referred as c-Ni) were finally dried in air at room temperature. The dried powders of both series of samples (uc-Ni and c-Ni) were annealed in different environments namely hydrogen and air at 973 K for 1 h.

The structure of the samples was studied with x-ray diffraction using a P.W. 1718 x-ray diffractometer with filtered Cu Kα radiation of wavelength $\lambda = 1.5418$ Å. Microstructure

[5] For Ni–Ag nanoparticles, Bala *et al* [21a] have reported in their paper that silver coating of Ni nanoparticles was accomplished by a simple transmetallation reaction [21b] wherein the Ni atoms residing on the surface of the Ni nanoparticles act as localized reducing agents for the silver ions in solution.

The reaction occurs since the redox potentials of Ni^0 oxidation and Ag^+ reduction are such that $Ni^0 + 2Ag^+ \rightarrow Ni^{2+} + 2Ag^0$ is a spontaneous reaction.

From the reported redox potentials we have

$$Ag^+ + e^- \rightarrow Ag^0 \qquad +0.80\ \text{V} \qquad \text{(i)}$$
$$Ni^{2+} + 2e^- \rightarrow Ni^0 \qquad -0.23\ \text{V}. \qquad \text{(ii)}$$

Therefore

$$Ni^0 + 2Ag^+ \rightarrow Ni^{2+} + 2Ag^0 \qquad +1.03\ \text{V} \qquad \text{(iii)}$$

is an energetically favourable reaction.

Thus the reduction of silver ions by Ni metal can proceed easily and this use of surface Ni atoms as a reducing agent obviates the need to employ any external reducing agent for Ag ions. A few layers of Ni atoms on the Ni core are consumed in the transmetallation reaction.

The methodology is general and may be extended to the formation of other nanoparticles core–shell systems. Bala *et al* have reported similar reaction for $Co_{core}Ag_{shell}$ nanoparticles also [13]. In both references [21a] and [13], the metal salt solution was first reduced by sodium borohydride ($NaBH_4$) to obtain the metal powder. Ag_2SO_4 solution was then added to the obtained nanoparticles and the coating accomplished via the transmetallation reaction.

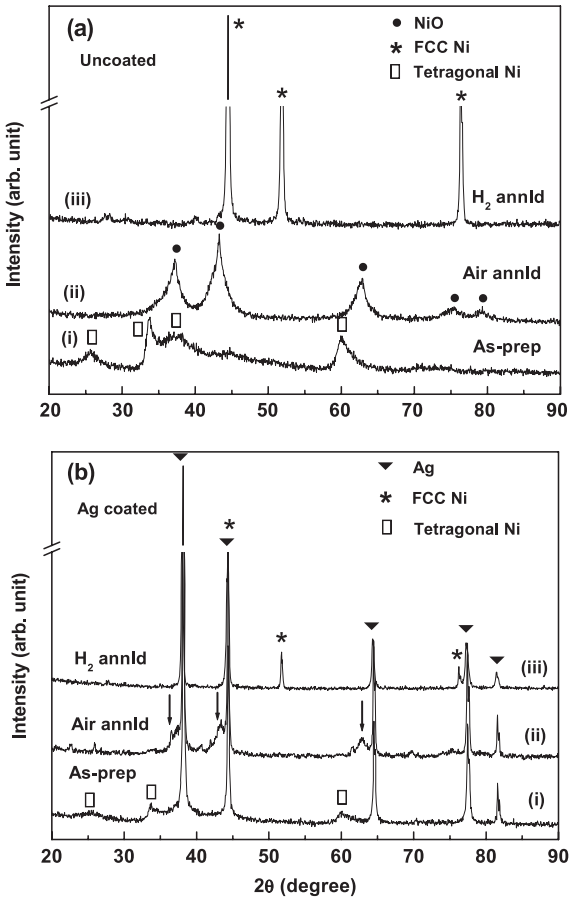

Figure 1. Powder XRD patterns of as-prepared, air annealed (at 973 K) and hydrogen annealed (at 973 K) particles of (a) uncoated Ni and (b) Ag coated Ni samples. The arrows in diffractogram (b)-(ii) indicate peaks of NiO.

was studied with a JEM 2000cx transmission electron microscope (TEM). *In situ* composition analysis has been done by EDAX (energy dispersive analysis of x-rays). The room temperature M–H (magnetization (M) versus field (H)) curves were measured with a vibrating sample magnetometer using magnetic fields up to 14 kOe. The low temperature magnetization measurements (M–H loop at 5 K and FC (field cooled)/ZFC (zero field cooled) curves) were done using a SQUID magnetometer with fields up to 50 kOe.

3. Results and discussion

3.1. X-ray diffraction and microstructure

Figure 1 shows the x-ray diffraction (XRD) patterns of as-prepared, air annealed and hydrogen annealed particles of uncoated and Ag coated Ni samples. The as-prepared uc-Ni sample (figure 1(a), diffractogram (i)) exhibits features that indicate a crystalline structure with some degree of disorder. The most intense peak in diffractogram 1(a)–(i) occurs at an interplanar spacing ('d') of 0.2667 nm and the second most intense at $d = 0.1543$ nm. In fcc Ni, the most intense (111) and the second most intense (200) peaks occur at interplanar spacings of 0.2034 and 0.1762 nm respectively. The XRD pattern of the end product of the borohydride reduction reaction thus does not correspond to fcc Ni. It does not correspond to NiO or any Ni–B

compound either, as vouched by the complete mismatch of the peak positions in diffractogram 1(a)–(i) with data available for NiO or Ni–B compounds in JCPDS (Joint Committee of Powder Diffraction Standards) files. We mention here that boron derivatives of the transition metal (here Ni) are often obtained as by-products in a borohydride reduction reaction, though a judicious choice of reaction conditions can prevent/minimize their formation[6]. As discussed in [19] and [20], through detailed calculations the pattern has been indexed to a tetragonal crystal structure with lattice parameters $a = 0.4920$ nm and $c = 0.5355$ nm. We have proposed that a tetragonal Ni–O_β lattice gets derived from the fcc Ni lattice by the incorporation of oxygen atoms at the interstitial positions of the latter. The dissolved oxygen atoms modify the fcc structure of virgin Ni particles, straining them into tetragonal lattice.

When this sample was annealed in air, surprisingly enough, evolution of fcc Ni was observed in the temperature range 573–773 K [19, 20]. Finally after annealing at 973 K broad NiO peaks appeared in the XRD pattern (figure 1(a), diffractogram (ii)), indicating transformation to nanocrystalline NiO phase. On the other hand, heat treatment in hydrogen at 973 K resulted in the emergence of pure fcc Ni peaks in the diffractogram (figure 1(a)-(iii)), implying that the as-prepared uncoated sample predominantly contains Ni. The disorder apparent in the diffraction pattern of the as-prepared sample thus gets removed on annealing, resulting in Ni reverting back to its usual fcc structure.

Similar annealing experiments were also carried out on the silver coated nickel particles for comparison of structural and magnetic properties. Figure 1(b) shows the XRD patterns of as-prepared and annealed samples of the Ni–Ag series. The as-prepared c-Ni sample exhibits a pattern (figure 1(b), diffractogram (i)) dominated by highly intense Ag peaks with only a feeble trace of tetragonal Ni, though this is rightly the phase encapsulated by the Ag shell as can clearly be understood from the preparation technique. The representative peaks of tetragonal Ni are not quite discernible in the as-prepared c-Ni sample. When this sample was annealed in air and hydrogen, peaks of NiO and fcc Ni respectively appeared in the diffractograms (figure 1(b), (ii) and (iii)) along with the usual peaks of silver. No change was observed in the XRD pattern of the H_2 annealed sample on annealing at a further higher temperature of 1173 K. The presence of individual Ni and Ag peaks even on annealing at 1173 K—a temperature close to the melting point of silver (1253 K)—further confirms the immiscibility of elemental Ni and Ag.

An important point to be noted is the dominating presence of Ag peaks in the XRD patterns of all three samples. This is primarily because Ag has a scattering factor nearly four times that of Ni [23], causing the resulting highly intense Ag peaks to nearly mask the peaks of Ni. A rather surprising observation is the presence of NiO peaks in the diffraction pattern of the air annealed c-Ni sample (figure 1(b), (ii)). This is quite contrary to expectations since the Ag shell is expected to act as a passivating layer and prevent any oxygen diffusion from air. However, possibly, the Ag shell becomes porous because of the mobility of the Ag atoms [24][7] on annealing the sample at a temperature as high as 973 K. This in turn allows oxygen diffusion to take place through this shell, resulting in the combination of these oxygen atoms with the encapsulated Ni, and the subsequent formation of NiO. It is important to mention here that

[6] Wells *et al* [22a] have shown for Fe nanoparticles prepared by this method that the use of borohydride solution of higher molarity results in low boron content in the sample. In their case the boron content *decreased* from 31 to 10 at.% on *increasing* the strength of $NaBH_4$ solution from 0.1 to 1 M. Likewise, Chen *et al* [22b] have reported for Co nanoparticles prepared by this method that a 10 M $NaBH_4$ solution produced pure Co nanoparticles whereas a 5 M $NaBH_4$ solution produced a mixture of Co and Co_2B as end product. It is worth mentioning in this context that our use of a higher molar concentration borohydride solution may be one of the reasons for the near absence of borides in our samples in accordance with the findings of Wells *et al* and Chen *et al*.

[7] During annealing, we can expect Ag to have a larger mobility than Ni since Ag has a lower melting point ($T_m = 961\,^\circ$C) than Ni ($T_m = 1453\,^\circ$C). At the annealing temperature of $T = 700\,^\circ$C, T/T_m are 0.728 and 0.482 for Ag and Ni respectively. This enables larger mobility of Ag atoms and hence gaps in the Ag shell.

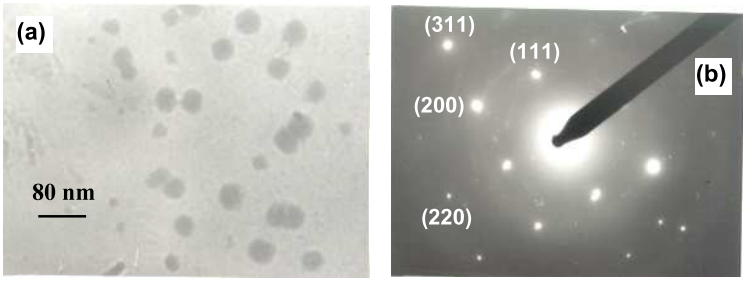

Figure 2. (a) TEM micrograph of as-prepared silver coated Ni particles with an average size of 44 nm. (b) Electron diffractogram of the same sample with Miller indices of Ag marked.

Table 1. Magnetic parameters of the M–H loops at 5 K for the *as-prepared* samples.

Sample	H_C (Oe)	M_R (emu g^{-1})	M at 50 kOe (emu g^{-1})
uc-Ni	900	19.5	78
c-Ni	300	4.6	40

though the two most common oxides of silver namely Ag_2O and AgO have some of their XRD peak positions close to those of NiO, they cannot exist in the 973 K air annealed c-Ni sample since they decompose into their constituent elements at 503 and 373 K respectively [25].

The EDAX analysis indicated the composition of the particles to be Ag 23.3 at.% and Ni 76.7 at.%. In terms of weight% this comes to Ni 64.2% and Ag 35.8%. The TEM micrograph of the as-prepared c-Ni sample shown in figure 2(a) indicates the formation of aggregated spherical particles of average diameter 44 nm. The spherical shape ensures that the particles are strain free and have negligible shape anisotropy. The selected area electron diffraction pattern (SAED) of these nanoparticles is shown in figure 2(b). The pattern is characteristic of polycrystalline particles. The rings could be indexed to the fcc Ag structure, with the numbers in brackets representing the Miller indices of different Ag planes. The SAED pattern did not show any reflection that could be associated with the core Ni nanoparticles. A possible explanation for this could be that the Ag shell is sufficiently thick and uniform and therefore prevents penetration of the electron beam to the Ni core and efficient electron scattering from it.

3.2. Magnetic properties

3.2.1. Results. Figure 3(a) shows the field variation of magnetization, i.e., M–H curves of the as-prepared coated and uncoated Ni samples at 300 K. These exhibit a linear behaviour with low magnetization values indicative of a paramagnetic (PM) state, while hysteresis with large values of magnetization is observed for the same samples at 5 K (figure 3(b)). Some differences are, however, apparent from the hysteresis loops in figure 3(b). While the uc-Ni sample shows large values of coercivity (H_C) and remnant magnetization (M_R) (table 1) with only a feeble tendency towards saturation, c-Ni exhibits lower values for these parameters with a clear tendency to saturate. The hysteresis and high magnetization values at 5 K suggest that both samples undergo transition from their room temperature (300 K) paramagnetic state to a different magnetic state, at some temperature intermediate to 5 and 300 K.

In order to further investigate the nature of this magnetic transition and the precise temperature of its occurrence, the magnetization (M) as a function of temperature (T) was measured in zero field cooled (ZFC) and field cooled (FC) conditions under an applied field

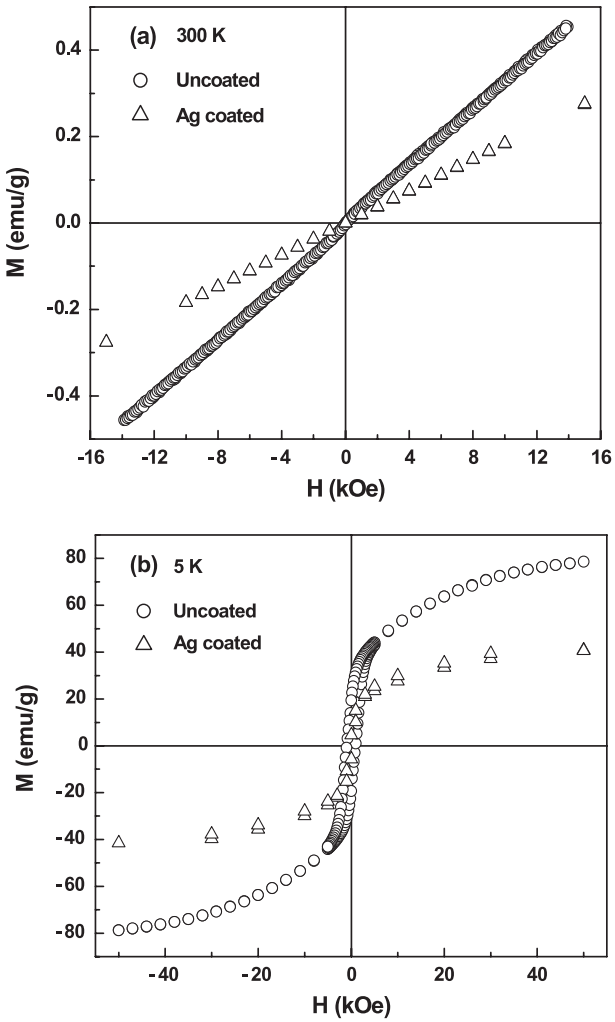

Figure 3. M–H plots of as-prepared c-Ni and uc-Ni samples at (a) 300 K and (b) 5 K.

of $H = 100$ Oe in the temperature range 5–300 K for uc-Ni and 5–80 K for c-Ni. As shown in figure 4 the ZFC magnetization curve of the uncoated and the Ag coated sample peaks respectively at $T_{max} = 20$ and 19 K and thereafter drops to zero, hinting at the metastable nature of the sample magnetization. On the other hand the FC magnetization curve continues to increase below T_{max} in the case of both samples, apparently distinguishing these systems from what is observed in canonical spin glasses. The strong irreversibility between the FC and ZFC branches at ∼20 K indicates that the magnetic transition occurs in the vicinity of this temperature. However, from these observations it cannot be concluded whether the observed transition is related to the superparamagnetic blocking of particle moments or their spin-glass-like freezing. Therefore for comparison and also for tracing the origin of this transition, magnetic measurements were performed on the samples annealed in air and hydrogen.

The room temperature magnetic isotherms (M–H plots) for the 973 K air annealed coated and uncoated Ni samples are shown in figure 5. At a first inspection the curves indicate a

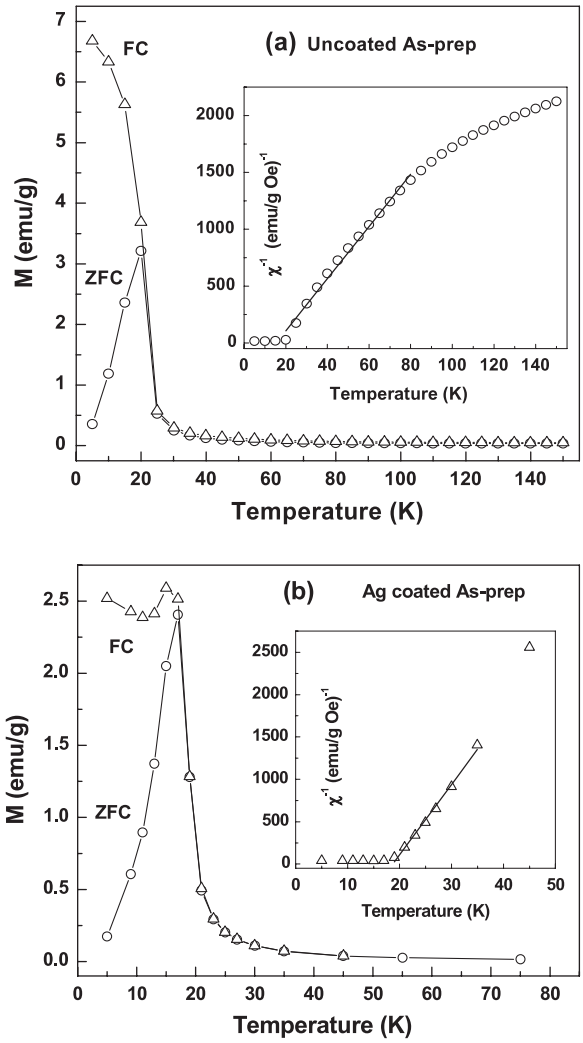

Figure 4. Field cooled (FC) and zero field cooled (ZFC) magnetization as a function of temperature at 100 Oe applied field for as-prepared Ni particles of (a) uncoated and (b) Ag coated samples. Insets: inverse susceptibility versus temperature plot fitted to the Curie–Weiss law.

typical non-hysteretic superparamagnetic behaviour which is due to the NiO component of these samples. However, an attempt to fit these curves to the simple Langevin function expected for a superparamagnet yielded poor results. Instead it is necessary to include an additional linear contribution χH to the magnetization in order to get reasonably good fits. We have therefore fitted the expression

$$M(a) = M_S \left[\coth(a) - \frac{1}{a} \right] + \chi H \tag{1}$$

in which M_S is the saturation magnetization, $a = \mu H / K_B T$, μ is the magnetic moment of a particle, K_B is Boltzmann constant and χ is the susceptibility. The values of M_S, μ and χ as obtained from the fit of the modified Langevin function (equation (1)) to the M–H curves are shown in table 2 and also in the insets of figure 5. It is worth mentioning that there are earlier reports about the M–H data for NiO [5] and Fe–Ni–B [26] nanoparticles being fitted to a modified Langevin function containing an extra linear term, though the reason for the inclusion of the linear term was not specified in these reports.

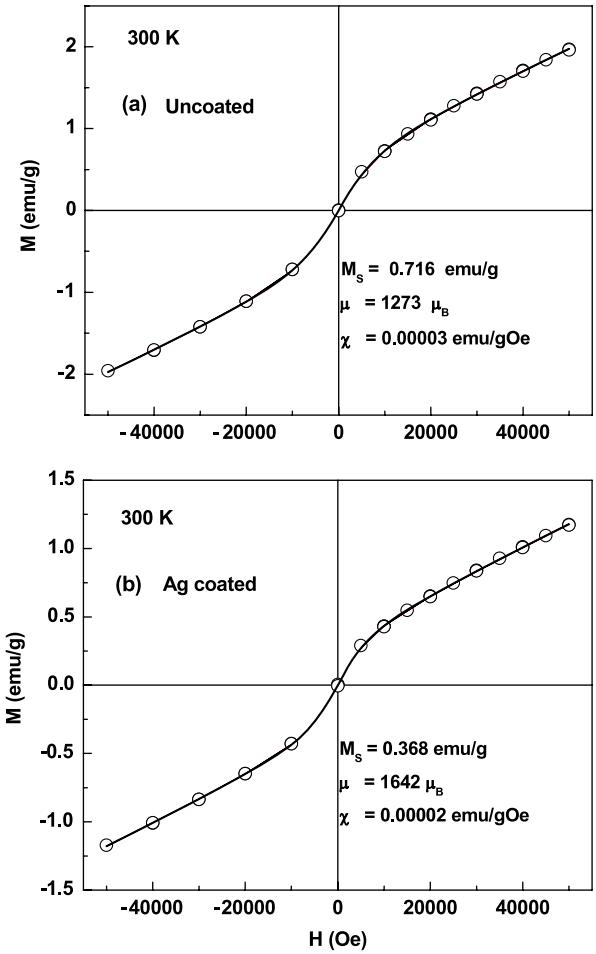

Figure 5. *M–H* plots at 300 K for the air annealed (at 973 K) samples of (a) uncoated and (b) Ag coated series. The bold line in both plots is the fit of the modified Langevin function (equation (1) in text) to the data. The insets give the magnitude of the fitting parameters as obtained from the fits.

Table 2. Magnetic parameters obtained from the fit of the modified Langevin function to the *M–H* curves at 300 K for the *air annealed* samples.

Sample	Particle moment, μ (μ_B)	Saturation magnetization, M_S (emu g^{-1})	Susceptibility (χ) (emu g^{-1} Oe^{-1})
uc-Ni	1273	0.716	0.000 03
c-Ni	1642	0.368	0.000 02

The temperature dependence of magnetization of the uncoated and Ag coated air annealed samples has been investigated through the FC and ZFC curves (figure 6), measured under a constant DC field of 100 Oe. Figure 6(a) shows these curves for the uncoated sample. Typical features of the blocking process of an assembly of superparamagnetic particles are seen with an average blocking temperature $T_B = 110$ K. This is defined as a temperature at which the ZFC curve exhibits a maximum. The ZFC peak is quite broad, hinting at the progressive blocking of the superparamagnetic particle moments with a distribution of relaxation times related to the distribution in particle size and the direction of anisotropy axis [26]. The silver coated Ni sample annealed in air at 973 K also shows a maximum in the ZFC curve but at a much higher

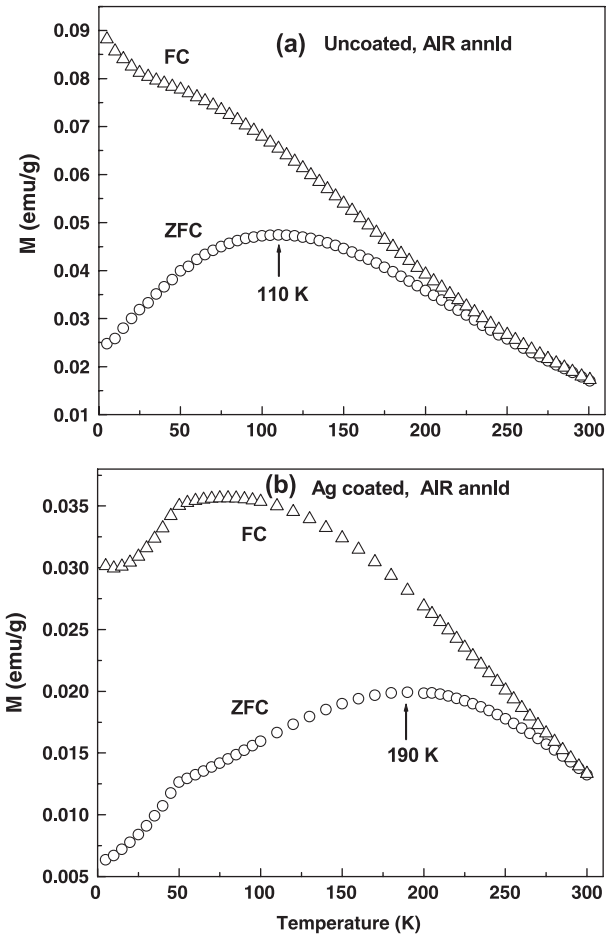

Figure 6. Field cooled and zero field cooled magnetization as a function of temperature at 100 Oe applied field for the 973 K air annealed particles of (a) uncoated and (b) Ag coated samples.

Table 3. Magnetic parameters of the M–H plot at 300 K for the *hydrogen annealed* samples.

Sample	M_S (emu g^{-1})	M_R (emu g^{-1})	H_C (Oe)
uc-Ni	37.17	4.5	54
c-Ni	15.68	1.5	58
Bulk Ni	54.4	–	6

temperature of 190 K. In both samples, T_B corresponds to the blocking temperature of the NiO component in them.

As regards the samples annealed in hydrogen, the room temperature M–H plots of the uncoated and Ag coated samples are shown in figure 7 and the corresponding magnetic parameters listed in table 3 along with those of bulk Ni. In contrast to the as-prepared samples which show paramagnetic response with magnetic field, the M–H plots of the hydrogen annealed samples exhibit hysteresis. This is expected since the XRD patterns of the hydrogen annealed samples show sharp fcc Ni peaks (figures 1(a) and (b), diffractogram (iii)). Yet, in spite of being constituted of pure fcc Ni, the magnitude of saturation magnetization M_S (37.17 emu g^{-1}) in case of the uc-Ni sample is about 31.6% less than that of bulk fcc Ni at 300 K.

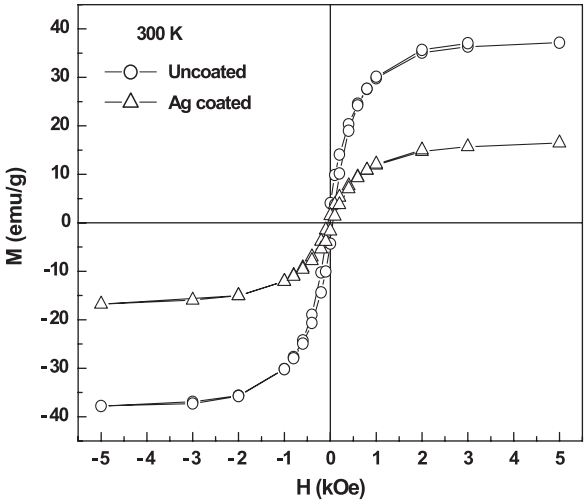

Figure 7. *M–H* plots at 300 K for (○) uncoated and (△) Ag coated samples annealed in hydrogen at 973 K.

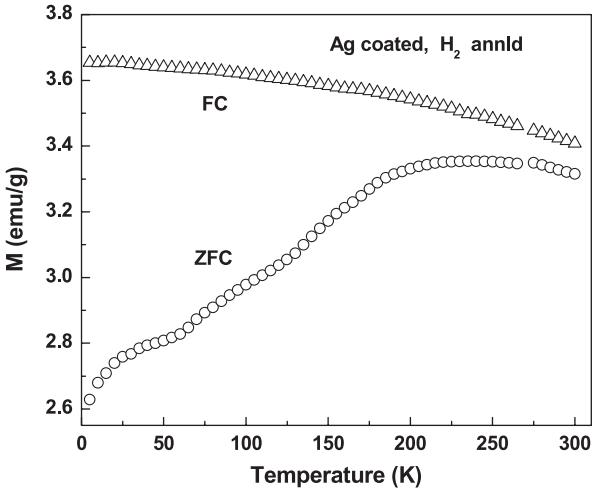

Figure 8. Field cooled and zero field cooled magnetization as a function of temperature at 100 Oe applied field for the Ag coated 973 K hydrogen annealed sample.

The *M–T* plots of the Ag coated sample exhibit a striking difference with bulk Ni. Although this sample shows ferromagnetic character at 300 K (like bulk Ni), the ZFC and FC magnetization curves instead of superposing, exhibit a split right from room temperature (figure 8)—a behaviour not expected for bulk Ni. However, such a behaviour may result from the encapsulated Ni cores (now fcc after H_2 annealing) of the particles which (cores) are large enough to be in a blocked state at 300 K. In other words the irreversibility in figure 8 is due to the particle nature of the sample and is characteristic of nanocrystalline Ni [17]. Similar FC/ZFC curves have also been reported earlier [27] in the case of uncoated nanocrystalline Ni.

3.2.2. Discussion.

3.2.2a. As-prepared samples. Some of the features observed in the present magnetic measurements of the as-prepared samples such as low magnetization values and non-hysteretic magnetization response in the *M–H* plots at 300 K, and very large values of magnetization in the hysteresis loops at 5 K, are rather puzzling. Roy *et al* have attributed these low values

of magnetization to the modified crystal structure of Ni where the presence of interstitial oxygen in the lattice generates 'superexchange' interactions. The combination of direct exchange and oxygen-mediated superexchange interactions between the Ni atoms eliminates Ni ferromagnetism [20], yielding a paramagnetic state of tetragonal Ni at room temperature. More specifically, a complete disruption of the spin configuration of the unit cell ensues, with each particle having a paramagnetic collection of atomic spins within it and hence no magnetic moment. Such a state is responsible for the low values of magnetization and a non-hysteretic response at 300 K in the as-prepared samples.

Coming to the low temperature magnetic state of both coated and uncoated as-prepared samples, it can be said that the bifurcation in the FC/ZFC curves of these samples at ∼20 K is a typical signature of the metastable nature of the magnetization and is exhibited by various magnetically disordered systems such as spin glasses, cluster glasses, superparamagnets and even inhomogeneous ferromagnets. In fact in case of single-domain fine particles, the maximum in the ZFC curve is roughly defined as blocking temperature T_B. T_B generally changes with change in the strength of interparticle dipolar interactions. This interaction strength depends on the distance between particles and hence on particle concentration, which may in turn be dependent on the molar concentration of the $NiCl_2$ solution from which the particles have been prepared. But no such change in the transition temperature of ∼20 K was observed when the M–T curves were repeated for samples prepared from $NiCl_2$ solution of different molar concentrations [28]. This rules out the possibility of 20 K being a blocking temperature of superparamagnetic particles.

The appearance of a maximum at 20 K in the ZFC curve of all as-prepared uncoated and silver coated Ni samples therefore suggests that the transition at 20 K is intrinsic to the system. It is independent of external parameters such as sample molarity and the presence/absence of Ag coating and may therefore owe its origin to the modified structure of the Ni lattice, i.e., oxygen-stabilized tetragonal Ni. This is quite logical since the peak at 20 K is present in the ZFC magnetization curve of only as-prepared samples and not air annealed or hydrogen annealed samples, none of which is constituted of tetragonal Ni. When AC susceptibility measurements on the as-prepared samples were carried out in a range of frequencies, no change was observed in the peak position at 20 K [29].

We attribute the peak at 20 K to a PM–FM (ferromagnet) phase transition involving the internal ordering of the spins inside each particle, whereby the hitherto paramagnetic oxygen-stabilized tetragonal Ni phase inside a particle becomes ferromagnetically ordered [29]. The reciprocal susceptibility plotted as a function of temperature (insets of figure 4) could be fitted to the Curie–Weiss law [$\chi = C/(T - \theta)$] for $T > T_{max}$ with an ordering temperature θ of ∼20 K. The positive sign of θ suggests the onset of strong ferromagnetic correlations and therefore corroborates our proposition. This FM ordering inside a particle imparts large magnetic moment to the particle. In the case of the uncoated sample, subsequent dipolar interactions between these macromoments lead to the occurrence of a spin-glass-like (SGL) transition at 20 K itself. On application of a magnetic field at 5 K the moments are rotated from their frozen directions and then aligned in the direction of the applied field, thereby leading to the large magnetization enhancement observed at this temperature [29]. Since such enhanced magnetization is also observed in the M–H plot of the c-Ni sample, the PM–FM ordering at 20 K and the subsequent SGL transition, occurs in this sample as well. It is interesting to point out here that the presence of a PM component in the M–H plots at 300 K and the peak at 20 K in ZFC curves, appear in all concentrations of as-prepared samples in the range of 0.1–2 M $NiCl_2$ precursor solution [28]. We therefore believe that it is the oxygen-stabilized tetragonal phase of Ni which gives rise to the above features (PM component and peak at 20 K) because of the disordered collection of spins in the unit cell.

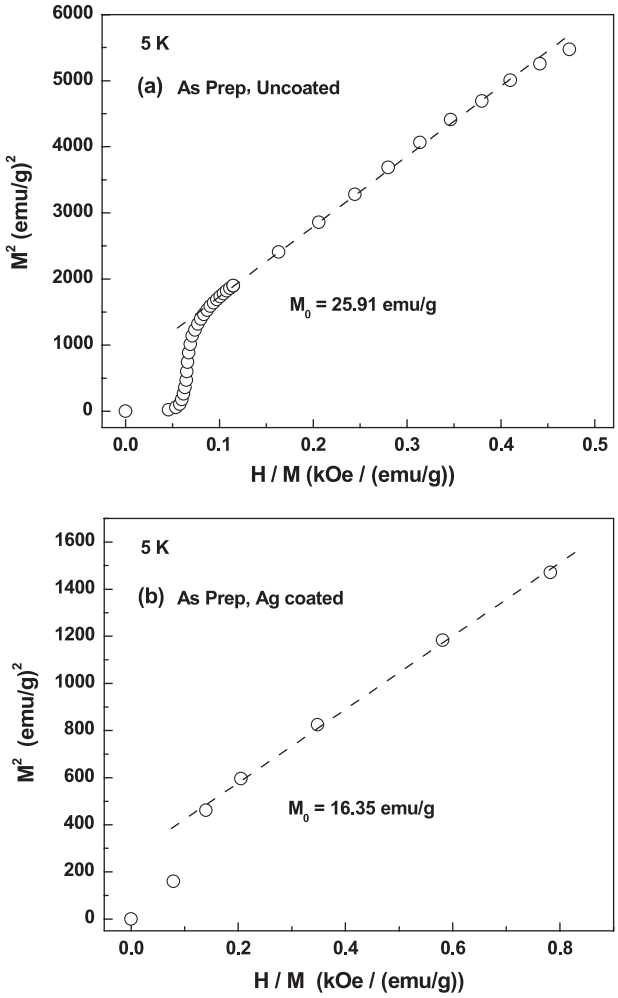

Figure 9. Arrott plots at 5 K for as-prepared particles of (a) uncoated Ni and (b) Ag coated Ni samples.

The smaller values of magnetization at 5 K in the case of the Ag coated sample is because of the presence of a substantial non-magnetic fraction in it. Since in ferromagnetic transition metals the 3d electrons are the main contributors to magnetism, the presence of the non-magnetic fraction implies a reduction in 3d electron population and therefore a corresponding change in magnetic behaviour. On the other hand the higher coercivity of the uc-Ni sample at 5 K (table 1) may be due to the pinning of the tetragonal core spins by the surface oxide spins (from the SSO layer) at the interface between the core and the surface. This prevents these interface-situated core spins from reversing their direction commensurate with the applied field, thereby resulting in appreciable magnetic anisotropy and hence large coercivity in this sample. In the Ag coated sample, the Ag shell prevents the formation of the spontaneous surface oxide layer. The absence of any pinning effect in this sample therefore results in a greatly reduced coercivity and remnant magnetization, with the net magnetization of the sample being dominated simply by the ordered tetragonal Ni core. From the Arrott plots shown in figure 9, the spontaneous magnetization M_0 at 5 K in the as-prepared state of uc and c-Ni has been estimated to be 26 and 16.35 emu g^{-1} respectively. The lower M_0 value in the case of c-Ni is again due to the absence of any contribution from the non-magnetic fraction of the sample.

3.2.2b. Air annealed samples. Contrasting values are observed for the fitting parameters (table 2) obtained by fitting the modified Langevin function to the room temperature (300 K) M–H plots of the air annealed samples. While the particle moment of the c-Ni sample is larger than the uc-Ni one, its saturation magnetization is smaller in comparison to the latter. We speculate the larger magnetic moment of the c-Ni sample to be due to a small ferromagnetically ordered fcc Ni core in each particle, which (core) escaped oxidation on annealing in air. The presence of this fcc Ni core is not discernible from the XRD pattern because of the masking of the fcc Ni peaks by highly intense Ag peaks. As regards the smaller saturation magnetization of the c-Ni sample it must be noted that since Ag is a heavy metal (at. wt 108 amu), each c-Ni particle is heavier than its uc-Ni counterpart so that the number of particles constituting 1 g of the c-Ni sample is small. Therefore the net contribution of these relatively few particles to the magnetization per gram of the sample is not substantial, even though their individual magnetic moment is higher than the uc-Ni particles. The Ag coated air annealed Ni particles can thus be summarized as being constituted of a small fcc Ni core, surrounded first by a NiO shell and then by the Ag shell. In contrast the uncoated air annealed particles are constituted only of NiO.

It has been observed that the inclusion of the linear term (χH) to the usual Langevin function is necessary only when the function is fitted to data taken up to high fields. Probably on application of a high magnetic field the uncompensated surface spins in the NiO component of the particles start aligning in tune with the field, giving rise to the paramagnetic component. Since the c-Ni sample has relatively small number of particles constituting 1 g of the sample, there are only few NiO regions per gram. In addition the extent of the NiO region in c-Ni is smaller in comparison to the uc-Ni sample since the latter is constituted only of NiO and has no fcc Ni component. Considering these facts the smaller susceptibility (χ) value of the c-Ni sample can logically be explained.

As a support to our proposition of the existence of an fcc Ni core in the particles of the c-Ni air annealed sample, the M–H plot of this sample at 5 K recorded after cooling in a field of 50 kOe is shown in figure 10. A shifted hysteresis loop with coercivity values of 3190 Oe (left) and 1445 Oe (right) is clearly seen. The loop is shifted leftwards by as much as 873 Oe. This phenomenon, termed as exchange anisotropy, is usually seen in the case of structures where a ferromagnetic and antiferromagnetic species are exchange coupled or when the magnetic environments of surface and core spins are different. The exchange interaction between the uncompensated surface spins of NiO and the fcc Ni core of the particles results in the shifted hysteresis loop in this sample.

To explain the difference in the magnitude of the blocking temperature for uncoated and Ag coated air annealed samples, we recall that in the uncoated sample the complete Ni gets converted to NiO on annealing in air at 973 K whereas in the Ag coated sample, part of the Ni stays unoxidized in each particle, implying the existence of an fcc Ni core in the particle. The exchange coupling between the ferromagnetic Ni core and the NiO shell in each particle causes the NiO spins close to the surface of the FM core to be pinned to it. The pinning effect imparts greater stability to the NiO moment and is responsible for the higher blocking temperature of NiO in case of the c-Ni sample. A kink is observed at 50 K in both the FC and ZFC magnetization curves of the c-Ni air annealed sample (figure 6(b)). We speculate this to be indicative of the blocking of the fcc Ni cores of the particles. However, AC susceptibility measurements are required for confirmation of this conjecture.

3.2.2c. Hydrogen annealed samples. The reasons for the reduction of M_S in the nanostate are (i) surface disorder or symmetry breaking effects at the surface and (ii) oxygen contamination. In the case of Ag coated Ni an additional reason might be surface alloying with non-magnetic

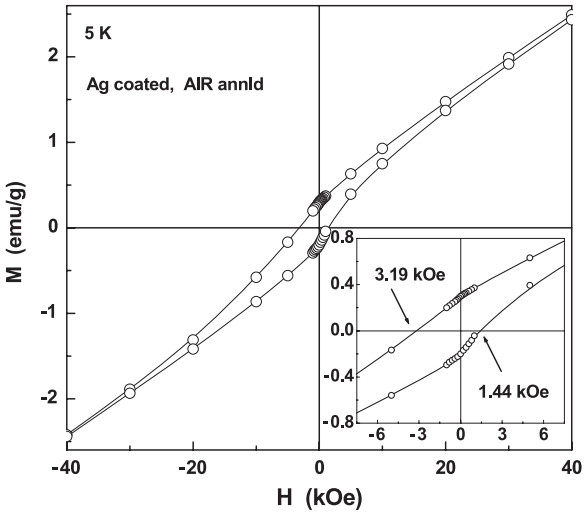

Figure 10. *M–H* plot at 5 K for the Ag coated air annealed sample after cooling in a field of 50 kOe. A shifted hysteresis loop is clearly seen.

silver atoms or an atomic level intermixing between Ag and Ni [15]. The M_S value of c-Ni (15.68 emu g^{-1}) is about 58% less than that of uc-Ni. This is attributed to the presence of the non-magnetic Ag fraction in the sample.

4. Conclusions

Ni–nickel oxide and Ni–Ag nanoparticles having core–shell morphology have been synthesized by a simple chemical route involving a $Ni^{2+} \rightarrow Ni$ reduction as the first step, followed by a transmetallation reaction $Ni + 2Ag^{+} \rightarrow 2Ag + Ni^{2+}$ in aqueous $AgNO_3$ solution at room temperature. The transmetallation reaction occurs at the surface of the Ni particles, replacing a small part of Ni with a surface layer of Ag. The structure and magnetic properties of the as-prepared and heat-treated (in different atmospheres) samples of both series have been investigated. The following conclusions could be drawn from the experimental observations.

(1) The as-prepared samples exhibit a crystal structure (tetragonal) different from the usual fcc structure of Ni, due to the presence of interstitial oxygen atoms in the Ni lattice.
(2) The Ag shell prevents the formation of the spontaneous surface oxide (SSO) layer in the as-prepared sample but is unable to prevent NiO formation on annealing the as-prepared sample in air at 973 K. This is because the Ag shell becomes porous at this temperature and allows oxygen diffusion through it.
(3) Both as-prepared *coated* and *uncoated* Ni samples undergo a magnetic transition close to 20 K. This has been identified as a PM to FM phase transition of the oxygen-stabilized tetragonal phase of the particles. The transition is thus independent of the presence/absence of Ag coating.
(4) The air annealed c-Ni sample has larger particle moment (μ) but smaller saturation magnetization (M_S), and also exhibits higher blocking temperature T_B in comparison to the air annealed uc-Ni sample. The larger magnetic moment is due to the presence of a small ferromagnetically ordered fcc Ni core in each particle while the higher T_B is due to the pinning of the NiO spins via exchange coupling between the fcc core and the NiO shell in each particle.
(5) The hydrogen annealed samples show lower saturation magnetization values compared to that of bulk Ni, even though they have Ni in its usual fcc form. The reduction in M_S

is due to surface disorder or symmetry breaking effects which is a common feature in nanoparticles.

Acknowledgment

The present work was partially supported by the Board of Research in Nuclear Sciences (BRNS), Department of Atomic Energy (DAE), Mumbai, India.

References

[1] Puntes V F, Krishnan K M and Alivisatos A P 2001 *Science* **291** 2115
[2] Murdock E S, Simmons R F and Davidson R 1992 *IEEE Trans. Magn.* **28** 3078
[3] Lu L, Sui M L and Lu K 2000 *Science* **287** 1463
[4] Kodama R H, Makhlouf S A and Berkowitz A E 1997 *Phys. Rev. Lett.* **79** 1393
[5] Makhlouf S A, Parker F T, Spada F E and Berkowitz A E 1997 *J. Appl. Phys.* **81** 5561
[6] Uchikoshi T, Sakka Y, Yoshitake M and Yoshihara K 1994 *Nanostruct. Mater.* **4** 199
[7] Zhang P, Zao F, Urban F K, Khabari A, Griffiths P and Hosseini-Tehrani A 1999 *J. Magn. Magn. Mater.* **195** 437
[8] Carpenter E E, Sims J A, Wienmann J A, Zhou W L and O'Connor C J 2000 *J. Appl. Phys.* **87** 5615
[9] Skumryev V, Stoyanov S, Zhang Y, Hadjipanayis G, Givord D and Nogues J 2003 *Nature* **423** 850
[10] Fonseca F C, Goya G F, Jardim R F, Muccillo R, Carreno N L V, Longo E and Leite E R 2002 *Phys. Rev.* B **66** 104406
[11] Jung J S, Choi K H, Chae W S, Kim Y R, Jun J H, Malkinski L, Kodenkandath T, Zhou W, Wiley J B and O'Connor C J 2003 *J. Phys. Chem. Solids* **64** 385
[12] Goya G F, Fonseca F C, Jardim R F, Muccillo R, Carreno N L V, Longo E and Leite E R 2003 *J. Appl. Phys.* **93** 6531
[13] Bala T, Arumugum S K, Pasricha R, Prasad B L V and Sastry M 2004 *J. Mater. Chem.* **14** 1057
[14] Kumar A, Damle C and Sastry M 2001 *Appl. Phys. Lett.* **79** 3314
[15] Sun L, He J H, Sheng H W, Searson P C, Chien C L and Ma E 2003 *J. Non-Cryst. Solids* **317** 164
[16] Xiao J Q, Jiang J S and Chien C L 1992 *Phys. Rev. Lett.* **68** 3749
[17] Nagamine L C C M, Mevel B, Dieny B, Rodmacq B, Regnard J R, Revenant Brizard C and Manzini I 1999 *J. Magn. Magn. Mater.* **195** 437
[18] He J H, Sheng H W, Schilling P J, Chien C L and Ma E 2001 *Phys. Rev. Lett.* **86** 2826
[19] Roy A, Srinivas V, Ram S, De Toro J A and Riveiro J M 2004 *J. Appl. Phys.* **96** 6782
[20] Roy A, Srinivas V, Ram S, De Toro J A and Mizutani U 2005 *Phys. Rev.* B **71** 184443
[21a] Bala T, Bhame S D, Joy P A, Prasad B L V and Sastry M 2004 *J. Mater. Chem.* **14** 2941
[21b] Park J and Cheon J W 2001 *J. Am. Chem. Soc.* **123** 5743
[22a] Wells S, Charles S W, Morup S, Linderoth S, van Wonterghem J, Larson J and Madsen M B 1989 *J. Phys.: Condens. Matter* **1** 8199
[22b] Chen J P, Sorensen C M, Klabunde K J and Hadjipanayis G C 1995 *Phys. Rev.* B **51** 11527
[23] Henke B L, Gullikson E M and Davis J C 1993 X-ray interactions: photoabsorption, scattering, transmission and reflection at $E = 5$–$30\,000$ eV, $Z = 1$–342 *At. Data Nucl. Data Tables* **54** 181
[24] Sandstrom P, Svedberg E B, Hohansson M P, Birch J and Sundgren J E 1999 *Thin Solid Films* **353** 166
[25] Lide D R (ed) 1991/1992 *CRC Handbook of Chemistry and Physics* 72nd edn (Boca Raton, FL: CRC Press) chapter 4, p 96
[26] De Biasi E, Ramos C A, Zysler R D and Romero H 2002 *Phys. Rev.* B **65** 144416
[27] Nayak B B, Vitta S, Nigam A K and Bahadur D 2006 *Thin Solid Films* **505** 109
[28] Roy A, Srinivas V, Ram S, De Toro J A and Goff J P 2006 *J. Appl. Phys.* **100** 094307
[29] Roy A, Srinivas V, De Toro J A and Goff J P 2006 *Phys. Rev.* B **74** 104402